

Article

# Charge Critical Phenomena in a Field Heterostructure with Two-Dimensional Crystal

Alexander L. Danilyuk, Denis A. Podryabinkin, Victor L. Shaposhnikov and Serghej L. Prischepa \* 

Department of Micro- and Nanoelectronics, Belarusian State University of Informatics and Radioelectronics, 220013 Minsk, Belarus; danilyuk@bsuir.by (A.L.D.); arm@tut.by (D.A.P.); shaposhnikov@bsuir.by (V.L.S.)

\* Correspondence: prischepa@bsuir.by

**Abstract:** The charge properties and regularities of mutual influence of the electro-physical parameters in a metal (M)/insulator (I)/two-dimensional crystal heterostructure were studied. In one case, the transition metal dichalcogenide (TMD) MoS<sub>2</sub> was considered as a two-dimensional crystal, and in another the Weyl semi-metal (WSM) ZrTe<sub>5</sub>, representative of a quasi-two-dimensional crystal was chosen for this purpose. By self-consistently solving the electrostatic equations of the heterostructures under consideration and the Fermi–Dirac distribution, the relationship between such parameters as the concentration of charge carriers, chemical potential, and quantum capacitance of the TMD (WSM), as well as the capacitance of the I layer and the interface capacitance I–TMD (WSM), and their dependence on the field electrode potential, have been derived. The conditions for the emergence of charge instability and the critical phenomena caused by it are also determined.

**Keywords:** field heterostructure; transition metal dichalcogenides; Weyl semi-metals; charge properties; charge instability; quantum capacitance; self-consistent solution

## 1. Introduction

Currently, the search for and study of promising materials with new properties for solid-state information storage and processing devices is actively underway. These include both two-dimensional (2D) semi-conductors [1–4] and materials with unusual electronic states, such as topological insulators and topological semi-metals [5–9]. Currently, 2D semi-conductors, with a particular focus on transition metal dichalcogenides (TMDs) and heterostructures on this basis, are emerging as serious candidates for future solid-state information processing and storage device technology [10]. Their potential consists in improved device scaling and energy-efficient switching compared to traditional bulk semi-conductors, such as Si, Ge and AIII–BV compounds [2]. These materials offer significant advantages, especially in ultra-thin devices of atomic thickness. Their unique structure makes it possible to create monatomic nano-ribbons, as well as vertical and lateral heterostructures. This versatility in design, combined with their distinctive properties, paves the way to efficient energy control in electronic devices.

Considerable attention has been drawn to topological semi-metals, which can be divided into three main groups: Weyl semi-metals (WSMs), Dirac semi-metals [7–9] and topological semi-metals with nodal lines [11–13]. In Dirac and Weyl semi-metals, two doubly degenerate bands or two non-degenerate bands, respectively, intersect at singular points or nodes near the chemical potential, forming four-fold degenerate Dirac points or doubly degenerate Weyl points, and diverge linearly in all three momentum directions. These correspond to low-energy excitations. The scale of self-energy is small, which creates prospects for the development of both energy-efficient information processing elements and ultra-sensitive sensors [7–9]. The features of the electronic structure of the topological materials are reflected in the electronic properties and lead to a number of unusual effects, such as extremely high magneto-resistance without a tendency to saturation, high mobility



**Citation:** Danilyuk, A.L.; Podryabinkin, D.A.; Shaposhnikov, V.L.; Prischepa, S.L. Charge Critical Phenomena in a Field Heterostructure with Two-Dimensional Crystal. *Solids* **2024**, *5*, 193–207. <https://doi.org/10.3390/solids5020013>

Academic Editor: Fabrizio Dolcini

Received: 15 February 2024

Revised: 11 March 2024

Accepted: 3 April 2024

Published: 6 April 2024



**Copyright:** © 2024 by the authors. Licensee MDPI, Basel, Switzerland. This article is an open access article distributed under the terms and conditions of the Creative Commons Attribution (CC BY) license (<https://creativecommons.org/licenses/by/4.0/>).

and low effective mass of current carriers, non-trivial Berry phase, chiral anomaly and anomalous Hall effect, and special behavior regarding optical conductivity [8,9]. The prospects of using TMD and magnetic WSM for spin-to-charge conversion, an important effect for spintronics [14,15], is also worth noting.

Along with numerous studies of the properties of the above materials, including ab initio calculations [6,10], little attention has previously been paid to the study of their charge properties, manifested in field heterostructures. Investigation of charge phenomena in metal M (field electrode)/insulator I/semi-conductor S field heterostructures (FHS MISs) is highly relevant, since they form the root of the elemental base of modern information processing and storage devices. 2D TMDs are promising in terms of replacing traditional silicon MIS transistors in information processing devices. Weyl semi-metals are of additional interest in terms of the study of non-trivial physical effects and phenomena in FHS MISs, which can be used to create information processing devices. In FHS MIS with 2D or quasi-2D materials, issues related to the study of electro-physical parameters, such as chemical potential, charge carrier concentration, quantum capacitance, and boundary state capacitances, as well as their mutual influence on each other, are important. The inter-relationships between electro-physical parameters with the parameters of heterostructures, as well as with the potential of the field electrode, are also very relevant. The influence of various factors on the electro-physical parameters will be significantly different compared to FHS MISs based on bulk semi-conductors. Such effects will be significantly more sensitive to the properties of materials and interfaces in the TMD-based FHS MISs [16]. This contributes to the manifestation of charge instability effects, hysteresis phenomena [16–19] caused by charge localization on defect states, and phase transitions [20]. On the one hand, this will affect the stability of FHS MISs, and on the other, it will contribute to the identification of new effects that can be exploited in the development of future generations of solid-state information processing devices. As for the studies of charge instabilities in FHS MISs with WSM, there are currently no systematic studies on this issue to the best of our knowledge. However, it is worth noting that, due to the presence of low energy electronic excitations in WSMs, similar effects in WSM-based FHS MISs should be manifested with a high degree of probability.

Thus, investigation of the mutual influence of the electro-physical parameters of FHS MISs with 2D TMDs and WSMs, considering the possibility of the occurrence of charge instabilities, is relevant. In this work, for the first time, the modeling of charge properties and charge instability in the M/I/2D TMD and quasi-2D WSM field heterostructures was carried out. The simulation was performed by self-consistent solution of the electrostatic equations and the Fermi–Dirac distribution. Self-consistent solutions have been obtained that relate the electrochemical potential, the concentration of conduction electrons and TMD (WSM) quantum capacitance as a function of the field electrode potential, insulator capacitance, and spectrum of the interface trap states. The occurrence of instability of quantum capacity and the critical phenomena caused by it are predicted.

## 2. Charge Properties. The Model

The electron concentration  $n_e$  in a 2D TMD per unit area is determined by the density of electronic states (DOSs)  $D(E)$  in the conduction band and chemical potential  $\chi$ , in accordance with the Fermi–Dirac statistics [16,21]

$$n_e(\chi) = \int_0^{\infty} D(E)f(E - \chi)dE, \quad (1)$$

where  $f$  is the Fermi–Dirac function and  $D(E)$  follows from ab initio calculations of band energy diagrams, and  $\chi = qU_c$  is the chemical potential defined from the electrostatic equation (see below). Here,  $q$  is the elementary charge, and the parameter  $U_c$  represents the voltage drop across the quantum capacitance  $C_Q$  [22]. The reference level for  $\chi$  is the middle of the semi-conductor band gap. Currently, to calculate the charge properties and

parameters of FHS MISs with 2D TMD, the following model density of electronic states of TMD is used [6,22,23]

$$D(E) = \frac{4\pi m_n}{h^2} \sum_n \Theta(E - E_n), \quad (2)$$

where  $\Theta$  is the Heaviside function,  $m_n$  is the effective mass of electrons,  $E_n$  is the energy of the  $n^{\text{th}}$  sub-band (the main contribution to the concentration of charge carriers comes from the ground state with  $n = 0$ ), and  $h$  is the Planck's constant.

For the concentration of conducting electrons in WSMs, we use Equation (1) and, for the DOS, we apply a two-band model with a negative band gap, described in [24,25]

$$D(E) = \frac{1}{\pi^2 h^3 v_F^2 c} \{ \Lambda(E, -\Delta) \Theta(E - \Delta) + [\Lambda(E, -\Delta) + \Lambda(-E, -\Delta)] \Theta(\Delta - E) \}, \quad (3)$$

where  $\Lambda(E, \Delta) = E\sqrt{E - \Delta}$ ,  $2\Delta$  is the energy band gap,  $v_F$  is the effective Fermi velocity, and  $c = (1/2m_n)^{1/2}$  is the parameter. The model described in [24,25] belongs to the minimum WSM model class [26]. For convenience of calculation, Equation (3) is transformed in such a way that the initially negative value  $\Delta$  is assumed to be positive.

Based on the condition of electro-neutrality of FHS MISs, the relationship between the chemical potential of a 2D semi-conductor or semi-metal, the concentration of charge carriers in them, the capacitance of the insulator, and the charge at the interface states, the potential of the field electrode is determined by the electro-statics equation, which for this case is written as [27–29]

$$qU_G = F_m - \zeta_s + \chi + \frac{q}{C_{ox}} [qn_e(\chi) + qn_t(\chi)], \quad (4)$$

where  $U_G$  is the potential of the field electrode,  $F_m$  is the work function of the field electrode material,  $\zeta_s$  is the electron affinity of the TMD (WSM),  $qn_t$  is the charge on trap states and  $C_{ox}$  is the capacitance of the insulating layer.

The relation between  $qn_t$  and the specific capacitance of trap states  $C_{it}$  has the well-known form [30,31],

$$C_{it} = \frac{d}{d\chi} (q^2 n_t(\chi)) \quad (5)$$

At  $F_m - \zeta_s = 0$  and constant density of trap states [27]

$$\chi \left( 1 + \frac{C_{it}}{C_{ox}} \right) + \frac{q^2 n_e(\chi)}{C_{ox}} = qU_G \quad (6)$$

The dependence of the charge of the trap states on the chemical potential is determined by the concentration of the occupied trap states  $n_t$  and their energy spectrum. In the case of a single energy level [31]

$$n_t(\chi) = \int \frac{N_t \delta(E - E_t) dE}{1 + g_n^{-1} \exp\left(\frac{E - \chi}{kT}\right)} = \frac{N_t}{1 + g_n^{-1} \exp\left(\frac{E_t - \chi}{kT}\right)}, \quad (7)$$

where  $N_t$  is the total concentration of traps,  $g_n$  is the degeneracy factor of trap state,  $E_t$  is the energy of trap state,  $k$  is the Boltzmann constant,  $T$  is the temperature, and  $\delta(E - E_t)$  is the Dirac delta function. In the case of Gauss distribution of trap energies [31]

$$n_t(\chi) = \int \frac{N_t dE}{1 + g_n^{-1} \exp\left(\frac{E - \chi}{kT}\right)} \frac{1}{(2\pi)^{1/2} \sigma_t} \exp\left[-\frac{(E - E_{tm})^2}{2\sigma_t^2}\right], \quad (8)$$

where  $E_{tm}$  is the energy corresponding to the maximum density of traps, and  $\sigma_t$  is the dispersion of distribution of traps energy.

The system of Equations (1)–(8) self-consistently determines the dependence of the concentration of charge carriers and  $\chi$  on  $U_G$ ,  $C_{ox}$  and  $C_{it}$ . Ultimately, it determines the self-consistent relationship of all electrical parameters of the FHS MIS with TMD or WSM. The quantum capacitance  $C_Q$ , in turn, is determined by the DOS and  $\chi$  according to [32].

$$C_Q = \int_0^{+\infty} D(E) \left( -\frac{df(E - \chi)}{dE} \right) dE, \quad (9)$$

In addition to quantum capacitance, important parameters are the field electrode-related capacitance  $C_G$  and the TMD (WSM)-related capacitance  $C_{CH}$ , which are also interrelated with charge carrier concentration and  $C_Q$ . In the low-frequency region, the indicated capacitances are expressed as follows [27]

$$C_G = \frac{C_Q + C_{it}}{1 + (C_Q + C_{it})/C_{ox}} \quad (10)$$

$$C_{CH} = \frac{C_Q}{1 + (C_Q + C_{it})/C_{ox}} \quad (11)$$

The joint solution of the system of Equations (1)–(11) allows us to trace the mutual influence of the electro-physical parameters of FHS MIS with a 2D semi-conductor or semi-metal and to identify the specific features of such mutual influence under conditions of charge instability.

### 3. Results and Discussion

#### 3.1. FHS MIS with TMD. Monoenergetic Traps

First, we consider the case of undoped TMD with monoenergetic traps characterized by a single energy level  $E_t$  located in the TMD band gap. The energy is measured from the top of the valence band. MoS<sub>2</sub> with a band gap of 1.86 eV is selected as TMD for calculations in this section. The total concentration of monoenergetic traps is defined as  $N_t$ . Self-consistent calculations of  $\chi$ ,  $n_e$ ,  $C_Q$ ,  $C_{it}$ ,  $C_G$ ,  $C_{CH}$  and electron charge on traps  $Q_t$  were carried out. Calculation of the above parameters of FHS MIS were performed depending on  $U_G$  and  $C_{ox} = \epsilon \epsilon_0/d$ . Here  $\epsilon$  is the relative dielectric permittivity,  $\epsilon_0$  is the vacuum permittivity and  $d$  is the insulating layer thickness. The  $C_{ox}$  value was chosen as equal to  $2 \times 10^{-3}$  F/m<sup>2</sup> (which corresponds to  $\epsilon = 7$ ,  $d = 30$  nm),  $N_t = 2 \times 10^{16}$  m<sup>-2</sup>, the  $E_t$  varied between 1.0 and 1.8 eV and the potential  $U_G$  between 0 and 5 V. Room temperature was considered,  $T = 300$  K.

The  $D(E)$  obtained from ab initio calculations was used to evaluate the  $n_e$ . For this structural optimization and electronic properties, calculations were performed employing the Vienna ab initio simulation package (VASP) [33] with the Perdew–Burke–Ernzerhof (PBE) exchange–correlation function [34]. A hybrid functional in the Heyd–Ernzerhof (HSE06) form was used to obtain more accurate band gaps [35]. The obtained DOS of the atomic monolayer MoS<sub>2</sub>, calculated with the approach developed in [33–35], is shown in the inset to Figure 1.

The results of self-consistent calculations revealed the following. Figure 1 shows the  $\chi(U_G)$  dependences at different states of  $E_t$ . As can be seen at  $E_t \leq 1.5$  eV, to achieve a self-consistent solution for the chemical potential of TMD in FHS MIS, the  $U_G$  value must be at least 1.1–1.6 V. Therefore, at  $E_t \leq 1.5$  eV and for  $U_G < 1.1$  V, there is no possibility of achieving any stable charge state of FHS MIS. The reason is an imbalance of local charges arising in the HS MIS, which does not allow achievement of the condition of electrical neutrality. This is since, to obtain the concentration of conduction electrons in MoS<sub>2</sub>, the chemical potential must be no lower than the middle of the band gap. Stable self-consistent solutions in this case exist at  $U_G > 1.1$ –1.6 V, when  $\chi$  exceeds a certain critical or threshold value (1.53 eV at  $E_t = 1.0$  eV and 1.6 eV at  $E_t = 1.5$  eV). Here, the chemical potential increases

non-linearly and monotonically, reaching the value of 1.75 eV with an increase in  $U_G$  to 4.0–4.5 V.

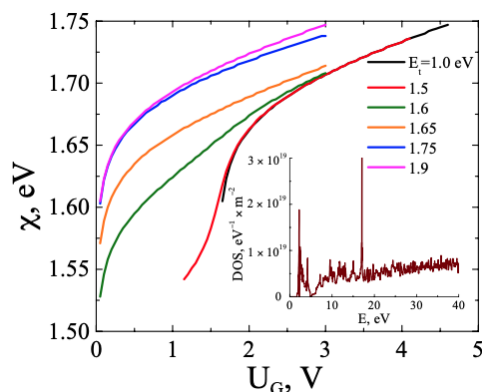


**Figure 1.** Chemical potential  $\chi$  of MoS<sub>2</sub> versus  $U_G$  of FHS MIS at different energy levels  $E_t$  of monoenergetic traps. Inset: DOS of the atomic monolayer MoS<sub>2</sub>.

With increasing energy of the monoenergetic trap, starting from  $E_t = 1.6$  eV, self-consistent solutions for  $\chi$  appear already from almost zero  $U_G$ . As can be seen from Figure 1, there is an increase in  $\chi$  at  $E_t = 1.6$  eV and 1.65 eV. Its values increase monotonically with increasing  $U_G$ , approaching the values of  $\chi$  for  $E_t = 1.0$  and 1.5 eV. At  $E_t \geq 1.75$  eV, the  $\chi$  values increase, and their maximum is achieved at lower  $U_G$  with respect to the case of smaller  $E_t$ . Further increase in the  $E_t$  (up to 1.8 eV) does not cause an increase in  $\chi$ .

The latter is associated with the approaching saturation of  $n_e$ , as follows from Figure 2a, where the dependences  $n_e$  versus  $U_G$  are shown. They are qualitatively similar to the dependences of  $\chi$  versus  $U_G$  and are characterized by an upward shift in  $U_G$  at  $E_t \leq 1.5$  eV.

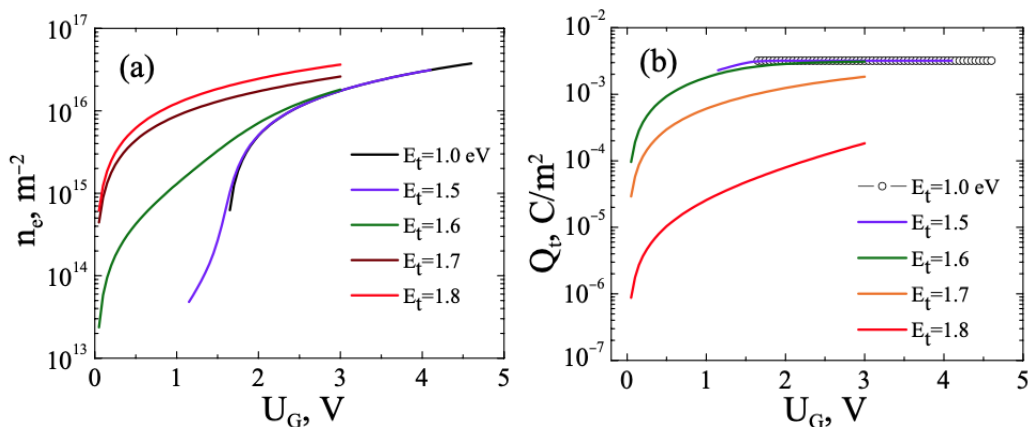


**Figure 2.** (a) Density of conduction electrons  $n_e$  versus  $U_G$  of FHS MIS at different energy levels  $E_t$  of monoenergetic traps; (b) electron charge on traps  $Q_t$  versus  $U_G$  of FHS MIS at different energy levels of  $E_t$  of monoenergetic traps.

Figure 2b shows the  $Q_t(U_G)$  dependences. In contrast to the charge created by conduction electrons, the charge localized on traps decreases with increasing trap energy, which is associated with the degree of occupation of trap states, which decreases when the trap is shallow relative to the bottom of the conduction band.

Figure 3a,b show the results of calculations of the dependences of the  $C_Q$ ,  $C_G$  and  $C_{CH}$  on  $U_G$  at two different values of  $E_t$  (1.5 eV, Figure 3a and 1.6 eV, Figure 3b). The  $C_Q(U_G)$  dependences are monotonic for both values of  $E_t$ . An increase in  $C_Q$  is observed with increasing  $U_G$  in accordance with the increase in  $n_e$  (see Figure 2a). The range of  $C_Q$  is 3–4 orders of magnitude.

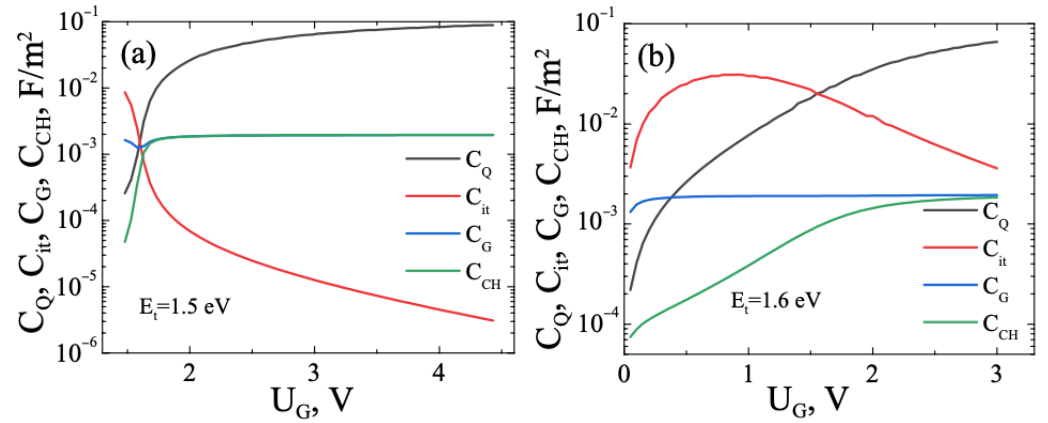


**Figure 3.** Quantum capacitance  $C_Q$ , capacitance of the I–TMD interface  $C_{it}$ , field electrode–TMD capacitance  $C_G$  and TMD capacitance  $C_{CH}$  versus  $U_G$  of FHS MIS at (a)  $E_t = 1.5$  eV and (b)  $E_t = 1.6$  eV.

At  $E_t = 1.0$  eV, the capacitance of the interface states that  $C_{it}$  sharply decreases, because the charge localized on the traps  $Q_t$  ceases to depend on potential  $U_G$  (see Figure 2b). In this case, as follows from Equations (10) and (11), the capacitance of the interface states does not affect the capacitances  $C_G$  and  $C_{CH}$ , which are now determined only by  $C_Q$  and  $C_{ox}$ .

As  $E_t$  approaches a value of 1.5 eV,  $C_{it}$  begins to influence the  $C_G$  and  $C_{CH}$  capacitances. From Figure 3a, it follows that, at  $E_t = 1.5$  eV, the  $C_{it}$  affects  $C_G$  and  $C_{CH}$  only in the region  $U_G = 1.5$ – $1.7$  V. In this region, we can assume that the charge system is not stable due to significant fluctuations in capacitances with a slight change in  $U_G$ . At  $E_t = 1.6$  eV,  $C_{it}$  increases significantly, becomes comparable to  $C_Q$ , and its dependence on  $U_G$  becomes non-monotonic with a maximum at  $U_G = 0.5$ – $1.0$  V (Figure 3b). This result is explained by the fact that the trap energy becomes comparable to the chemical potential. Therefore, at  $\chi \approx E_t$ , there is an increase in  $C_{it}$  with an increase in  $U_G$ . We also demonstrated that, at  $E_t > 1.7$  eV, there is a sharp decline in  $C_{it}$ .

Thus, in the presence of electronic trap states with a monoenergetic level, their influence on the stability of the charge state of FHS MIS is determined by the relationship between the chemical potential and the energy of the traps. For the case of relatively deep traps with an energy of 1.0–1.5 eV, unstable charge states arise in the  $U_G$  range up to a certain threshold value. This is because there are no conditions for the emergence of a charge balance, determined by the electrical neutrality condition of FHS MIS and the Fermi–Dirac statistics, which determine the  $n_e(\chi)$  dependence. The  $\chi$  value in turn is determined by  $U_G$ ,  $C_{ox}$  and  $Q_t$ . Such an imbalance does not allow self-consistency of the chemical potential, the concentration of conduction electrons, the charge on the traps, and the charge created by the field electrode. With increasing  $E_t$ , when the energy of traps becomes comparable to the value of  $\chi$ , non-linear charge effects arise, which also lead to instability of charge properties in the  $U_G$  range up to 2 V. This is due to an increase in the  $C_{it}$  which, in turn, is caused by the charge localized on the traps.

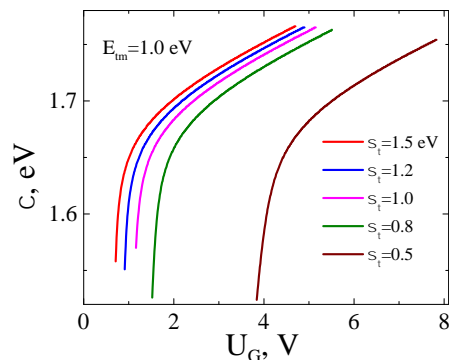
Finally, we should stress that the results obtained in this section for FHS MIS with MoS<sub>2</sub> as TMD are qualitatively valid for other TMDs, such as, e.g., MoSe<sub>2</sub>, MoTe<sub>2</sub>, WS<sub>2</sub>, WSe<sub>2</sub> and WTe<sub>2</sub>.

### 3.2. FHS MIS with TMD. Gauss Distribution for Trap Energies at the TMD–I Interface

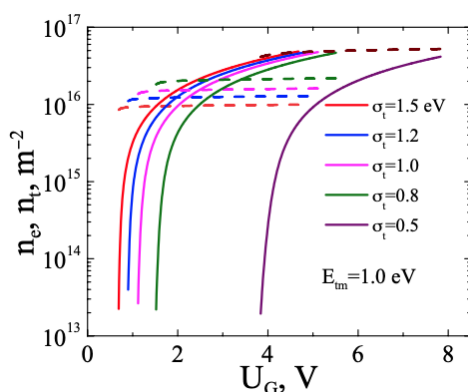
In this section we consider the spectrum of trap states at the TMD–I interface, assuming that the energy of the states is distributed according to the Gaussian law (Equation (8)). Calculations of  $\chi$ ,  $n_e$ ,  $n_t$ ,  $C_Q$ ,  $C_G$ ,  $C_{CH}$  were carried out for traps in molybdenum sulfite with the following parameters:  $T = 300$  K,  $E_{tm} = 0.8$ – $1.2$  eV,  $\sigma_t = 0.5$ – $1.5$  eV,  $N_t = 2 \times 10^{16}$  m<sup>-2</sup>.

Figure 4 shows the  $\chi(U_G)$  and Figure 5 the dependences of  $n_e$  and  $n_t$  on  $U_G$  at  $E_{tm} = 1.0$  eV. In this case, self-consistent solutions for  $\chi$  and  $n_e$  exist within a certain range of  $U_G$ . They arise only when  $U_G$  is greater than a threshold value  $U_{Gth}$ . Thus, at

$\sigma_t = 0.8\text{--}1.5$  eV,  $U_{Gth}$  is 0.7–1.53 V, and at  $\sigma_t = 0.5$  eV, the  $U_{Gth}$  shift reaches 4 V. Below these thresholds, there is no self-consistent solution and thus charge balance is not achieved. Therefore, we can consider the range  $U_G \leq U_{Gth}$  to be a range of charge instability. A decrease in  $\sigma_t$  shifts  $\chi$  and  $n_e$  towards higher  $U_G$  values. A decrease in  $E_{tm}$ , on the contrary, shifts these quantities towards lower  $U_G$ .



**Figure 4.** Chemical potential  $\chi$  of MoS<sub>2</sub> versus  $U_G$  of FHS MIS at different dispersion  $\sigma_t$  of Gauss distribution of traps energy.



**Figure 5.** Density of conduction electrons  $n_e$  (solid lines) and density of electrons localized in traps  $n_t$  (dashed lines) versus  $U_G$  of FHS MIS at different dispersion  $\sigma_t$  of Gauss distribution of traps energy.

The values of  $\chi$  are in the range 1.5–1.8 eV, and the range of  $n_e$  is  $10^{13}\text{--}5 \times 10^{16} \text{ m}^{-2}$ . The latter can be considered as a saturation value for  $n_e$ . In addition, a sharp rise occurs in the region of 0.5–2.0 V (at  $\sigma_t = 0.8\text{--}1.5$  eV), followed by a smoother transition to saturation. The concentration of electrons localized in traps changes slightly with increasing  $U_G$ ; it increases with a decrease in  $\sigma_t$  at a constant value of  $E_{tm}$ , from  $0.9 \times 10^{16}$  to  $2 \times 10^{16} \text{ m}^{-2}$ .

Figure 6a,b show the dependences of  $C_Q$ ,  $C_G$  and  $C_{CH}$  on  $U_G$ . The results of Figure 6a were obtained for the following set of the model parameters:  $\sigma_t = 0.8$  eV,  $E_{tm} = 1.0$  eV,  $C_{ox} = 2 \times 10^{-3} \text{ F/m}^2$ . In Figure 6b, these parameters were slightly changed, namely,  $\sigma_t = 0.75$  eV,  $E_{tm} = 1.05$  eV,  $C_{ox} = 3.54 \times 10^{-3} \text{ F/m}^2$ . Two types of behavior of  $C_Q$  versus  $U_G$  have been identified: monotonic change and abrupt change. The first type is observed in the region  $U_G = 1.5\text{--}2.0$  V and is associated with the presence of an exponential change in  $C_Q$ , leading to modulation of capacitances  $C_G$  and  $C_{CH}$  (Figure 6a). At the same time, the capacitance  $C_{it}$  does not practically change with increasing  $U_G$ . However, its contribution significantly affects the change in  $C_G$  and  $C_{CH}$  in the range  $U_G = 1.5\text{--}2.0$  V. For these  $U_G$  values, the change in  $C_G$  and  $C_{CH}$  reaches several times, which indirectly confirms the presence of charge instability.

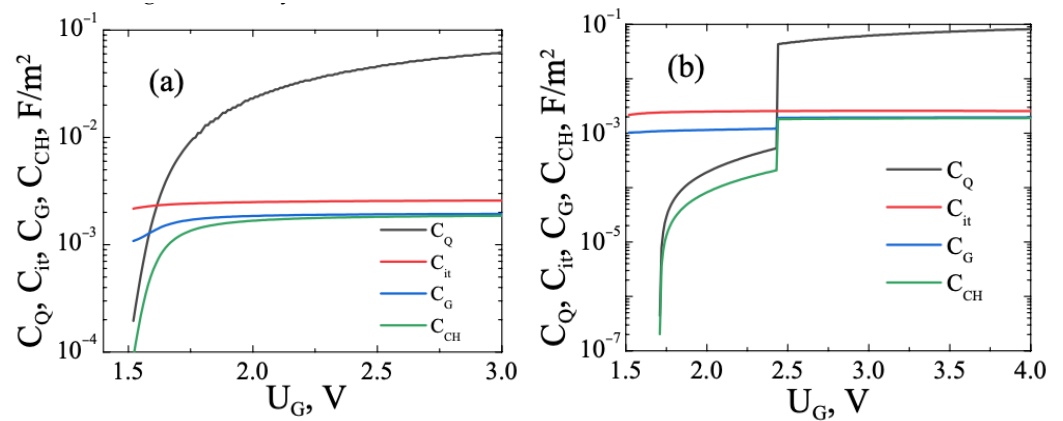


**Figure 6.** (a,b) Quantum capacitance  $C_Q$ , capacitance of the I-TMD interface  $C_{it}$ , field electrode–TMD capacitance  $C_G$ , and TMD capacitance  $C_{CH}$  versus  $U_G$  of FHS MIS in the case of Gauss distribution of traps energy at two slightly different sets of model parameters. For details, see the text. Inset to (b): Density of conduction electrons  $n_e$  versus chemical potential  $\chi$  for  $MoS_2$ .

Our calculation also revealed that, for larger values of  $\sigma_t = 1.5$  eV, the value of  $C_{it}$  does not exceed  $10^{-3}$   $F/m^2$  and the capacitances  $C_G$  and  $C_{CH}$  are determined only by  $C_Q$ . Moreover, they are close in value to each other in the entire  $U_G$  range. This is due to a decrease in concentration  $n_t$  at  $\sigma_t = 1.5$  eV (see Figure 5).

The second type of dependence is shown in Figure 6b. Slight variation in the parameters of the model leads, at  $U_G = 2.43$  V, to the appearance of two roots for  $C_Q$  in solving the system of Equations (1), (4), (5), (8) and (9). This causes a jump-like dependence of  $C_Q$  at  $U_G = 2.43$  V, and the value of  $C_Q$  changes by almost two orders of magnitude (from  $5.1 \times 10^{-4}$  to  $0.044$   $F/m^2$ ). The capacitance  $C_Q$  also shifts towards larger  $U_G$  at small values below  $10^{-3}$   $F/m^2$  and then, due to a jump, its value is restored, reaching a value with exponential growth, compared with Figure 6a. A reverse calculation of the electron concentration based on the jump-like dependence  $C_Q(\chi)$  showed that a similar jump occurs for the dependence  $n_e(\chi)$  (see inset to Figure 6b). This also confirms the conclusion regarding the instability of the charge in FHS MIS with  $MoS_2$  at some critical relationships of its electro-physical parameters.

Note that, in the case of Gaussian distribution, in contrast to the monoenergetic traps, when instability arises due to a decrease in  $E_t$ , the presence of a broadening of the energy spectrum of trap states leads practically to insensitivity of the capacitance  $C_{it}$  to the growth of  $U_G$ , remaining almost constant under the conditions considered. This leads to the fact that the capacitances  $C_G$  and  $C_{CH}$  are determined mainly by the behavior of  $C_Q$ . The situation becomes different when an abrupt change in  $C_Q$  and, accordingly, in the electron concentration occurs. If, in the previous cases, a self-consistent solution was absent at certain values of  $U_G$  and this was associated with the presence of instability, then here the manifestation of instability may mean that the relationships and mutual influence of the electro-physical parameters of FHS MIS are characterized by the presence of bi-stable states. This bi-stability characterizes the insulator–semi-conductor transition. Its mechanism is associated, in our opinion, with the influence of charge fluctuations leading to a transition between two states of a bi-stable system at a critical (threshold) value of  $U_G$ . An increase in charge fluctuations at a critical value of  $U_G$  in this case leads to a switching of states of the bi-stable system by analogy with the phenomenon of noise-induced stochastic resonance [36].

The results obtained for two types of trap states described in Sections 3.1 and 3.2 in the general case can be explained as follows. Self-consistent solutions for  $\chi$  and  $n_e$  arise at certain threshold values of  $U_G$ , when a charge balance in the heterostructure determined by the Fermi–Dirac statistics and the electrical neutrality condition considering the charge on trap states is achieved. For  $U_G = 0$  V, when there is no positive charge created by the field electrode potential, the chemical potential is in the middle of the band gap. In this

case, in the presence of traps that capture only electrons, charge balance is not achieved, since the presence of a positive charge created by the field electrode is necessary. Physically, this is because an increase in the charge on traps leads to a mismatch between the electrical neutrality condition and the Fermi–Dirac statistics at a certain value of the potential  $U_G$ , due to the absence of an increase in the DOS with energy. This is why charge imbalance arises. Self-consistency is reached only with a certain increase in  $\chi$  above the energy of the middle of the band gap due to the action of the field electrode charge. This threshold effect is similar to the insulator–semi-conductor transition. Such transitions belong to the critical phenomena. They occur at critical values of some parameters of FHS MISs with TMD. In other words, we can assume the existence of critical points at which the charge balance is disrupted and the relationships between electro-physical parameters undergo qualitative changes.

### 3.3. FHS MIS with WSM

Weyl semi-metals are materials in which the valence band and conduction band intersect at separate points called Weyl nodes, causing a negative band gap. When the Fermi energy is near these nodes, the electrons effectively behave as relativistic Weyl fermions with linear energy dispersion and well-defined chirality. At present, a sufficient number of materials related to WSM is already known. It is worth mentioning that these include TaAs, NbAs, TaP, NbP, WTe<sub>2</sub>, MoTe<sub>2</sub> [6,7,37–39], a magnetic WSM SrRuO<sub>3</sub> [40–42], etc. In this work, we chose ZrTe<sub>5</sub>, which is considered as a WSM [24,25,37]. Like many other topological semi-metals, ZrTe<sub>5</sub> possesses small intrinsic energy scales.

The case of low temperature due to the presence of low-energy excitations in the WSM is discussed. In the region of high temperatures, the features are leveled out by thermal fluctuations. Anisotropic ZrTe<sub>5</sub> material with an orthorhombic *Cmcm* phase of ZrTe<sub>5</sub>, characterized by a parabolic dispersion around the  $2\Delta$  band gap, which transforms into a linear dispersion at higher energies, corresponds to the *a*–*c* plane. The dispersion along the *b* direction remains parabolic at all energies. Free electron-like behavior is assumed in the *b* direction. In addition, ZrTe<sub>5</sub> is characterized by the following parameters:  $v_F = 4.9 \times 10^5$  m/s,  $\Delta = 3$  meV,  $m_n = m_b = (1.8\text{--}2.0) m_0$  [24,25]. This semi-metal is also characterized by high mobility  $(1\text{--}4.5) \times 10^5$  cm<sup>2</sup>/V·s at low temperature, and effective masses in various directions are  $m_a = \Delta/v_a^2 = 0.001 m_0$ ,  $m_c = \Delta/v_c^2 = 0.0025 m_0$ . Here,  $m_0$  is the mass of a free electron, the masses  $m_a$ ,  $m_c$  and velocities  $v_a$ ,  $v_c$  correspond to directions in the *a*–*c* planes, and the mass  $m_b$  corresponds to the direction along the *b* axis.

For FHS MIS with ZrTe<sub>5</sub>, the case of distribution of trap states with a constant density according to Equation (6) was considered. Then, the capacitance of interface states  $C_{it}$  acts as a model parameter. Its value varied in the range  $C_{it} = (0\text{--}3)C_{ox}$ . In addition to those indicated above for ZrTe<sub>5</sub>, the following parameters were used for simulation:  $T = 0.2$  K and  $0.8$  K,  $\varepsilon = 16$ ,  $d = 40$  nm,  $C_{ox} = 3.54 \times 10^{-3}$  F/m<sup>2</sup>,  $U_G = 0.002\text{--}0.5$  V. Note also that the calculations were carried out for quasi-2D ZrTe<sub>5</sub>.

Figure 7 shows the DOS calculated from Equation (3) for  $\Delta = 3$  and  $6$  meV. In this model, the WSM phase has two Weyl points in the Brillouin zone, where the energy disappears,  $(k_a, k_c, k_b) = (0, 0, \pm\Delta^{1/2}/\hbar c)$  and, for negative band gap, the conditions for the minimal WSM model are fulfilled [26]. As follows from Figure 7, the DOS are monotonic and are characterized by the presence of kinks, at which the form of the  $D(E)$  dependence changes. Calculation of the  $\chi(U_G)$  dependences for various values of  $C_{it}$  revealed that they are qualitatively similar to the DOS, i.e., are also characterized by the presence of kinks (see inset to Figure 8). The value of  $\chi$  varies in the range  $5 \times 10^{-4}\text{--}0.5$  eV depending on the  $U_G$  potential and increases with its growth. The kink point shifts towards larger  $U_G$  as  $C_{it}$  increases.

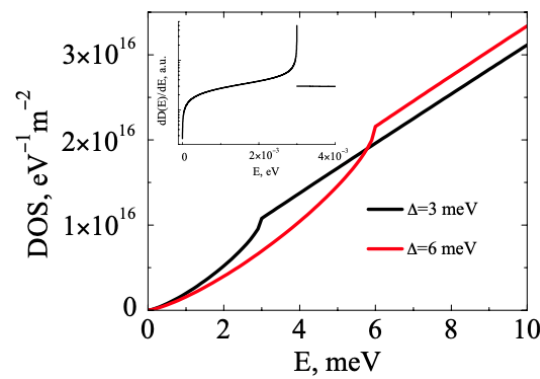


**Figure 7.** Density of states DOS of ZrTe<sub>2</sub> at two energy gap values. Inset: The first derivative of DOS versus energy for ZrTe<sub>5</sub> at  $\Delta = 3$  meV.

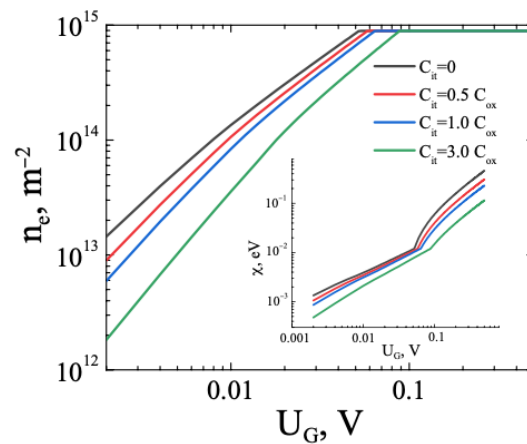


**Figure 8.** Density of conduction electrons  $n_e$  versus  $U_G$  of FHS MIS at different values of the capacitance of the I-WSM interface  $C_{it}$ . Inset: Chemical potential of ZrTe<sub>5</sub> versus  $U_G$  of FHS MIS at different values of the capacitance of the I-WSM interface  $C_{it}$ .

Figure 8 shows the concentration of conduction electrons as a function of  $U_G$ . As can be seen, they are characterized by an exponential rise to a threshold value  $U_{Gth}$ , after which they sharply move to saturation, at around  $10^{15} \text{ m}^{-2}$ . The capacitance  $C_{it}$  affects the threshold value  $U_{Gth}$ . With increasing  $C_{it}$ , the  $U_{Gth}$  value shifts towards higher  $U_G$ , similarly to the  $\chi(U_G)$  dependence. The saturation of  $n_e(U_G)$  in this case is associated with the fact that, after the break point, the DOS of the WSM depends linearly on energy. This leads, in the region of ultra-low temperatures, where the Fermi–Dirac function has a stepwise character, to the fact that, at  $U_G > U_{Gth}$ , when the chemical potential exceeds the energy, linear increase in DOS is compensated. As a result, the concentration is saturated with an almost constant value. At  $U_G < U_{Gth}$  where there is an increase in  $n_e$ , the DOS depends parabolically on the energy  $E$  and  $\chi$  becomes comparable to  $E$ .

Figure 9 shows the results of calculations of  $C_Q$  and  $C_G$  at  $T = 0.2$  K and  $C_{it} = 3.0 C_{ox}$ . The calculations of  $C_Q$  revealed the presence of oscillations accompanied by their compaction near  $U_{Gth}$  and a decrease in amplitude for  $C_G$  to  $(2.9 \pm 0.3) \times 10^{-3} \text{ F/m}^2$ . Our results also revealed that oscillations of  $C_Q$  are observed at any values of  $C_{it}$ , and their amplitude reaches 4 orders of magnitude ( $10^{-6}$ – $10^{-2} \text{ F/m}^2$ ). As  $C_{it}$  increases, the frequency of oscillations along  $U_G$  increases, and a compaction in oscillations is observed closer to the  $U_{Gth}$ . When the electron concentration reaches saturation,  $C_Q$  drops sharply to almost zero. This affects the  $C_G$  and  $C_{CH}$  capacitances. In this case, the capacitance  $C_G$  stabilizes at  $U_G > U_{Gth}$  due to the prevalence of constant capacitance  $C_{it}$ . A decrease in the amplitude of  $C_G$  oscillations is also observed at  $U_G < U_{Gth}$ : up to  $(2 \pm 1) \times 10^{-3} \text{ F/m}^2$  at  $C_{it} = 0.5 C_{ox}$  and up to  $(2.13 \pm 0.87) \times 10^{-3} \text{ F/m}^2$  at  $C_{it} = 1.0 C_{ox}$ .

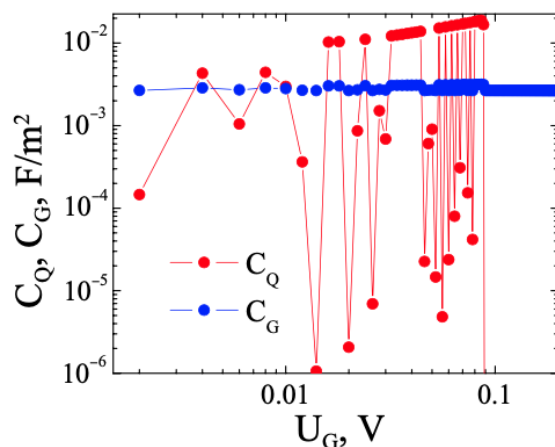


**Figure 9.** Quantum capacitance  $C_Q$  of ZrTe<sub>5</sub> and field electrode–WSM capacitance  $C_G$  versus  $U_G$  of FHS MIS.  $T = 0.2$  K.

The occurrence of such  $C_Q$  oscillations, which characterizes the presence of charge instability in the FHS MIS with WSM, can be associated with low excitation energies of the electronic system, the non-linearity of the dependence of the concentration of electrons excited by the  $U_G$  field, and the presence of a dispersion transition from a parabolic behavior to a linear one, which leads to the emergence of additional relatively small kinks in the  $\chi(U_G)$  and  $n_e(U_G)$  dependences.

When the temperature increases to 0.8 K, leveling of oscillations of  $C_Q$  and, accordingly, of  $C_G$  and  $C_{CH}$  is observed (Figure 10). In this case,  $C_Q$ ,  $C_G$ ,  $C_{CH}$  versus  $U_G$  values grow up to a certain threshold value of  $U_G$ , after which the  $C_Q$  and  $C_{CH}$  disappear, and the  $C_G$  stabilizes at  $C_{it} > 0$ .

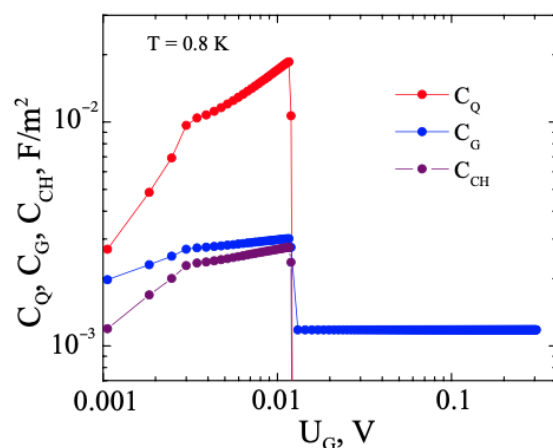


**Figure 10.** Quantum capacitance  $C_Q$  of ZrTe<sub>5</sub>, field electrode–WSM capacitance  $C_G$  and WSM capacitance  $C_{CH}$  versus  $U_G$  of FHS MIS.  $T = 0.8$  K.

Such radical change of  $C_Q(U_G)$  dependence with temperature is most likely due to a change of the Fermi–Dirac distribution. In fact, the broadening of the Fermi–Dirac function,  $f[(E-\chi)/kT]$ , and, accordingly, its derivative with respect to energy, which determines  $C_Q$ , significantly depends on  $T$ . At  $T = 0.2$  K, the broadening is very small and approaches the  $\delta$ -function, which contributes to the formation of a set of discrete, non-overlapping bursts of the derivative  $f[(E-\chi)/kT]$  in energy. This peculiar spectrum of the derivative ultimately leads to  $C_Q$  oscillations. With increasing temperature, the broadening of the derivative  $df[(E-\chi)/kT]/dE$  increases and such bursts overlap, smoothing out the discrete spectrum, which leads to the suppression of  $C_Q$  oscillations.

The obtained behaviors for FHS MIS with WSM can be associated primarily with the features of the band structure of ZrTe<sub>5</sub>, i.e., the presence of energy bands with linear and parabolic dispersion [24].

Currently, various mechanisms for instabilities in WSM have been proposed [42–47]. In the systems in which the filled valence band is in contact with the conduction band, the instability can be caused by gapless excitations around the zero-energy manifold, which are characterized by a smaller dimension compared to the spatial dimension of the system itself [43]. Instabilities induced by a magnetic field are also considered [44,45] and, in addition to the traditional Dyakonov–Shur instability for plasmons, entropy wave instability was discovered [46]. Instability of Weyl semi-metals against Coulomb interaction could also contribute [47,48].

However, in the case under consideration, within the framework of the model used, the occurrence of charge instability, in our opinion, should be associated with the influence of the following factors. The first issue is the presence of a kink at  $E = \Delta$  in the DOS, caused by a change in the dispersion law. This leads to the appearance of fluctuations of  $C_Q$  due to the transition from one dispersion law to another, which has a jump-like character. This fact is illustrated in the inset to Figure 7, which shows the derivative of the DOS versus the energy for  $\Delta = 3$  meV. As can be seen at  $E = \Delta$ , a discontinuity of the derivative is observed, which indicates a significant increase in fluctuations when approaching the  $E = \Delta$  region. This is also indicated by the derivative of the electron concentration versus the chemical potential, which is characterized by the presence of sharp rises and falls.

The second issue is that, when approaching  $T = 0$ , at which the Fermi–Dirac function tends to a stepwise form, but has not yet become so strict, the FHS MIS with ZrTe<sub>5</sub> charge system may lose stability due to the fact that an increase in the interface capacitance leads to a mismatch between the electrical neutrality condition and the Fermi–Dirac statistics at an energy close to the  $\chi$  value. This is since, near  $E = \Delta$ , the dispersion law will deviate from the parabolic towards a sharper increase in the DOS with energy. Therefore, as the  $C_{it}$  increases, the effect of increasing the oscillation frequency occurs when approaching the threshold value of the field electrode potential, at which saturation emerges, and the quantum capacitance decreases to zero.

#### 4. Conclusions

Simulation of the charge properties of FHS MIS with undoped monolayer MoS<sub>2</sub> with electron traps, characterized by such electro-physical parameters as chemical potential, conduction electron concentration, quantum capacitance, the capacitance of the TMD–I interface, the capacitance of the M–TMD and capacitance of the TMD, revealed the presence of charge instability in certain ranges of the field electrode potential. Regularities of changes in these parameters depending on the potential of the field electrode have been established for monoenergetic and Gaussian energy distributions of traps at the TMD–I interface. It is shown that, in the presence of electronic trap states with a monoenergetic level, their influence on the stability of the charge state of FHS MISs with MoS<sub>2</sub> is determined by the relationship between  $\chi$  and  $E_t$ . For the case of relatively deep traps with  $E_t = 1.0$ – $1.5$  eV, unstable charge states arise, which disappear when  $U_G > U_{Gth}$ . For shallow traps this threshold disappears, and an unstable charge state does not arise for all positive  $U_G$ . Such behavior is associated with the dependence of  $C_{it}$  on  $U_G$ ; it decreases along with increase in  $U_G$  in the case of deep traps and increases in the case of relatively shallow traps.

With the Gaussian distribution, due to the presence of broadening of the energy spectrum of trap states,  $C_{it}$  does not change significantly with  $U_G$  in the studied range, which determines the effect on the charge properties of FHS MIS with MoS<sub>2</sub>. It has been established that, in this case, an abrupt change in  $C_Q$  and  $n_e$  is also possible. We explain this instability by the emergence of bi-stability in the system. This bi-stability characterizes the insulator–semi-conductor transition. Its mechanism is associated, in our opinion, with the influence of charge fluctuations leading to a transition between two states of a bi-stable system at a critical (threshold) value of the field electrode potential. An increase in

charge fluctuations leads to a switching of states of a bi-stable system by analogy with the phenomenon of noise-induced stochastic resonance.

The results obtained for two types of trap states are explained by the fact that self-consistent solutions for  $\chi$  and  $n_e$  arise at certain threshold values of  $U_G$ , when the charge balance in the heterostructure is achieved, determined by the Fermi–Dirac statistics and the electrical neutrality condition, considering the charge on the trap states. Physically, this is because an increase in the charge on traps leads to a mismatch between the electrical neutrality condition and the Fermi–Dirac statistics at a certain value of the potential  $U_G$  due to the absence of an increase in the DOS with energy. As a result, a charge imbalance arises, and self-consistency is reached only at a certain growth of  $\chi$  above the energy of the middle of the band gap, due to the action of the field electrode charge. This threshold effect is similar to the insulator–semi-conductor transition. Such transitions belong to critical phenomena in which the charge balance is disrupted and the relationships between electro-physical parameters undergo qualitative changes. Our results correlate qualitatively with available experimental data, which show the presence of instability and hysteresis phenomena in transistor structures based on 2D TMD [49–53].

For FHS MIS with ZrTe<sub>5</sub>, the case of low temperature and a uniform energy spectrum of trap states, characterized by their capacitance, was considered. The presence of kinks in the dependence of  $\chi$  and  $n_e$  versus  $U_G$  in the range 0.05–0.09 V was revealed, arising due to a peculiarity in the DOS, which is characterized by a change in the dispersion law for electronic states from parabolic to linear. The  $n_e$  is characterized by reaching saturation at the kink point. The capacitance of the trap states in this case leads to a shift in the kink point along the field electrode potential.

The regularities of the influence of the  $C_{it}$  on the  $C_Q(U_G)$  dependence have been established. It is shown that, at  $T = 0.2$  K, oscillations of  $C_Q$  are observed at any values of the capacitance of interface states, the amplitude of which reaches four orders of magnitude, as well as a sharp drop in the region where  $n_e$  reaches saturation. With  $C_{it}$  increase, an increase in the frequency of  $C_Q$  oscillations is observed. The occurrence of such oscillations is associated with the non-linearity of the  $n_e(U_G)$  dependence, the presence of a transition of dispersion from parabolic to linear, which leads to the occurrence of charge fluctuations against the background of low excitation energies of the electronic system. An increase in temperature to 0.8 K leads to the disappearance of  $C_Q$  oscillations.

Thus, within the framework of the model used, the obtained behavior for FHS MIS with ZrTe<sub>5</sub> is associated with the peculiarities of its band structure, namely, the presence of energy bands with transitions between linear and parabolic dispersion. The obtained charge instability is due to two reasons. The first is the presence of a break in the DOS caused by a change in the dispersion law. This leads to the appearance of charge fluctuations of  $C_Q$  due to the transition from one dispersion law to another, which has a jump-like character. This is confirmed by the presence of discontinuity of the derivative of the DOS, leading to a significant increase in such fluctuations in the break region. The second issue is determined by the stepwise form of the Fermi–Dirac function, due to which an increase in the interface capacitance leads to a mismatch between the electrical neutrality condition and the Fermi–Dirac statistics at an energy close to the value of  $\chi$ , since near the break in the DOS the dispersion law will deviate from the parabolic law towards a sharper increase in the DOS, which leads to a charge imbalance, accompanied by the effect of compaction of oscillations.

**Author Contributions:** Conceptualization, A.L.D. and S.L.P.; Methodology, D.A.P.; Software, V.L.S.; Validation, V.L.S.; Formal analysis, D.A.P.; Investigation, A.L.D.; Writing—original draft, A.L.D.; Writing—review & editing, S.L.P.; Supervision, S.L.P. All authors have read and agreed to the published version of the manuscript.

**Funding:** This research was partially funded by the Belarussian Republic Foundation for Basic Research, grant F23RNF-159.

**Data Availability Statement:** The data presented in this study are available on request from the corresponding author due to ethical reasons.

**Acknowledgments:** ALD and DAP acknowledge financial support from the Belarussian Republic Foundation for Basic Research (grant F23RNF-159).

**Conflicts of Interest:** The authors declare no conflicts of interest.

## References

1. Huang, X.; Liu, C.; Zhou, P. 2D semiconductors for specific electronic applications: From device to system. *npj 2D Mater. Appl.* **2022**, *6*, 51. [[CrossRef](#)]
2. Nandan, K.; Agarwal, A.; Bhowmick, S.; Chauhan, Y.S. Two-dimensional semiconductors based field-effect transistors: Review of major milestones and challenges. *Front. Electron. Sec. Nano Microelectron.* **2023**, *4*, 127779. [[CrossRef](#)]
3. Liu, C.; Chen, H.; Wang, S.; Liu, O.; Jiang, Y.-G.; Zvarg, D.W.; Liu, M.; Zhou, P. Two-dimensional materials for next-generation computing technologies. *Nat. Nanotechnol.* **2020**, *15*, 545–557. [[CrossRef](#)] [[PubMed](#)]
4. Wei, T.; Han, Z.; Zhong, X.; Xiao, Q.; Liu, T.; Xiang, D. Two dimensional semiconducting materials for ultimately scaled transistors. *iScience* **2022**, *25*, 105160. [[CrossRef](#)]
5. Vergniory, M.G.; Elcoro, L.; Felser, C.; Regnault, N.; Bernevig, B.A.; Wang, Z. A complete catalogue of high-quality topological materials. *Nature* **2019**, *566*, 480–485. [[CrossRef](#)] [[PubMed](#)]
6. Naher, M.I.; Naqib, S.H. An ab-initio study on structural, elastic, electronic, bonding, thermal, and optical properties of topological Weyl semimetal TaX (X = P, As). *Sci. Rep.* **2021**, *11*, 5592. [[CrossRef](#)] [[PubMed](#)]
7. Armitage, N.P.; Mele, E.J.; Vishwanath, A. Weyl and Dirac semimetals in three-dimensional solids. *Rev. Mod. Phys.* **2018**, *90*, 015001. [[CrossRef](#)]
8. Bernevig, A.; Weng, H.; Fang, Z.; Dai, X. Recent progress in the study of topological semimetals. *J. Phys. Soc. Jpn.* **2018**, *87*, 041001. [[CrossRef](#)]
9. Lv, B.Q.; Qian, T.; Ding, H. Experimental perspective on three-dimensional topological semimetals. *Rev. Mod. Phys.* **2021**, *93*, 025002. [[CrossRef](#)]
10. Krivosheeva, A.V.; Shaposhnikov, V.L.; Borisenko, V.E.; Lazzari, J.-L. Heterostructures of two-dimensional transition metal dichalcogenides: Formation, ab initio modelling and possible applications. *Mater. Today Proc.* **2022**, *54 Pt 1*, 73–79. [[CrossRef](#)]
11. Yang, M.-X.; Luo, W.; Chen, W. Quantum transport in topological nodal-line semimetals. *Adv. Phys. X* **2022**, *7*, 2065216. [[CrossRef](#)]
12. Burkov, A.A.; Hook, M.D.; Balents, L. Topological nodal semimetals. *Phys. Rev. B* **2011**, *84*, 235126. [[CrossRef](#)]
13. Bi, R.; Yan, Z.; Lu, L.; Wang, Z. Nodal-knot semimetals. *Phys. Rev. B* **2017**, *96*, 201305. [[CrossRef](#)]
14. Han, W.; Otani, Y.; Maekawa, S. Quantum materials for spin and charge conversion. *npj Quant Mater.* **2018**, *3*, 27. [[CrossRef](#)]
15. Zhang, S.S.L.; Burkov, A.A.; Martin, I.; Heinonen, O.G. Spin-to-Charge Conversion in Magnetic Weyl Semimetals. *Phys. Rev. Lett.* **2019**, *123*, 187201. [[CrossRef](#)] [[PubMed](#)]
16. Makovskaya, T.I.; Danilyuk, A.L.; Krivosheeva, A.V.; Shaposhnikov, V.L.; Borisenko, V.E. Charge properties of the MOS transistor structure with the channel made from a two-dimensional crystal. *Russ. Microelectron.* **2020**, *49*, 507–515. [[CrossRef](#)]
17. Kaushik, N.; Mackenzie, D.M.A.; Thakar, K.; Goyal, N.; Mukherjee, B.; Boggild, P.; Petersen, D.H.; Lodha, S. Reversible hysteresis inversion in MoS<sub>2</sub> field effect transistors. *npj 2D Mater. Appl.* **2017**, *1*, 34. [[CrossRef](#)]
18. Late, D.J.; Liu, B.; Matte, H.S.S.R.; Dravid, V.P.; Rao, C.N. Hysteresis in single-layer MoS<sub>2</sub> field effect transistors. *ACS Nano*, **2012**; *6*, 5635–5641. [[CrossRef](#)]
19. Shu, J.P.; Wu, G.; Guo, Y.; Liu, B.; Wei, X.; Chen, Q. The intrinsic origin of hysteresis in MoS<sub>2</sub> field effect transistors. *Nanoscale* **2016**, *8*, 3049–3056. [[CrossRef](#)] [[PubMed](#)]
20. Lin, Y.-C.; Dumcenco, D.O.; Huang, Y.-S.; Suenaga, K. Atomic mechanism of the semiconducting-to-metallic phase transition in single-layered MoS<sub>2</sub>. *Nat. Nanotechnol.* **2014**, *9*, 391–396. [[CrossRef](#)] [[PubMed](#)]
21. Das, S.; Sebastian, A.; Pop, E.; McClellan, C.J.; Franklin, A.D.; Grasser, T.; Knobloch, T.; Illarionov, Y.; Penumatcha, A.V.; Appenzeller, J.Z.; et al. Transistors based on two-dimensional materials for future integrated circuits. *Nat. Electron.* **2021**, *4*, 786–799. [[CrossRef](#)]
22. Jiménez, D. Drift-diffusion model for single layer transition metal dichalcogenide field-effect transistors. *Appl. Phys. Lett.* **2012**, *101*, 243501. [[CrossRef](#)]
23. Cao, W.; Kang, J.; Liu, W.; Banerjee, K. A Compact Current-Voltage Model for 2D Semiconductor Based Field-Effect Transistors Considering Interface Traps, Mobility Degradation, and Inefficient Doping Effect. *IEEE Trans. Electron Devices* **2014**, *61*, 4282–4290. [[CrossRef](#)]
24. Martino, E.; Crassee, I.; Eguchi, G.; Santos-Cottin, D.; Zhong, R.D.; Gu, G.D.; Berger, H.; Rukelj, Z.; Orlita, M.; Homes, C.C.; et al. Two-Dimensional Conical Dispersion in ZrTe<sub>5</sub> Evidenced by Optical Spectroscopy. *Phys. Rev. Lett.* **2019**, *122*, 217402. [[CrossRef](#)] [[PubMed](#)]
25. Rukelj, Z.; Homes, C.C.; Orlita, M.; Akrap, A. Distinguishing the gapped and Weyl semimetal scenario in ZrTe<sub>5</sub>: Insights from an effective two-band model. *Phys. Rev. B* **2020**, *102*, 125201. [[CrossRef](#)]
26. McCormick, T.M.; Kimchi, I.; Trivedi, N. Minimal models for topological Weyl semimetals. *Phys. Rev. B* **2017**, *95*, 075133. [[CrossRef](#)]

27. Zebrev, G.I. Graphene Field Effect Transistors: Diffusion-Drift Theory. In *Physics and Applications of Graphene—Theory*; Mikhailov, S., Ed.; IntechOpen, Rijeka, Croatia, 2011; Chapter 23, pp. 475–498. [[CrossRef](#)]
28. Marin, E.G.; Bader, S.J.; Jena, D. A New Holistic Model of 2-D Semiconductor FETs. *IEEE Trans. Electron Devices* **2018**, *65*, 1239–1245. [[CrossRef](#)]
29. Najam, F.; Tan, M.L.P.; Ismail, R.; Yu, Y.S. Two-dimensional (2D) transition metal dichalcogenide semiconductor field-effect transistors: The interface trap density extraction and compact model. *Semicond. Sci. Technol.* **2015**, *30*, 075010. [[CrossRef](#)]
30. Sze, S.M.; Ng, K.K. *Physics of Semiconductor Devices*, 3rd ed.; John Wiley & Sons, Inc.: Hoboken, NJ, USA, 2008; 826p.
31. Kao, K.-C.; Hwang, W. *Electrical Transport in Solids with Particular Reference to Organic Semiconductors*; Pergamon Press: Oxford, UK, 1981; 663p.
32. Luryi, S. Quantum Capacitance Devices. *Appl. Phys. Lett.* **1988**, *52*, 501–503. [[CrossRef](#)]
33. Kresse, G.; Furthmüller, J. Efficient iterative schemes for ab initio total-energy calculations using a plane-wave basis set. *Phys. Rev. B* **1996**, *54*, 11169. [[CrossRef](#)] [[PubMed](#)]
34. Perdew, J.P.; Burke, K.; Ernzerhof, M. Generalized gradient approximation made simple. *Phys. Rev. Lett.* **1996**, *77*, 3865–3868, Erratum in *Phys. Rev. Lett.* **1997**, *78*, 1396. [[CrossRef](#)] [[PubMed](#)]
35. Heyd, J.; Scuseria, G.E.; Ernzerhof, M. Hybrid functionals based on a screened Coulomb potential. *J. Chem. Phys.* **2003**, *118*, 8207–8215. [[CrossRef](#)]
36. Anishchenko, V.S.; Neiman, A.B.; Moss, F.; Shimansky-Geier, L. Stochastic resonance: Noise-enhanced order. *Physics-Uspokhi* **1999**, *42*, 7–36. [[CrossRef](#)]
37. Liang, T.; Lin, J.; Gibson, Q.; Kushwaha, S.; Liu, M.; Wang, W.; Xiong, H.; Sobota, J.A.; Hashimoto, M.; Kirchmann, P.S.; et al. Anomalous Hall effect in ZrTe<sub>5</sub>. *Nat. Phys.* **2018**, *14*, 451–455. [[CrossRef](#)]
38. Zheng, H.; Hasan, M.Z. Quasiparticle interference on type-I and type-II Weyl semimetal surfaces: A review. *Adv. Phys. X* **2018**, *3*, 1466661. [[CrossRef](#)]
39. Sun, Y.; Wu, S.-C.; Ali, M.N.; Felser, C.; Yan, B. Prediction of Weyl semimetal in orthorhombic MoTe<sub>2</sub>. *Phys. Rev. B* **2015**, *92*, 161107. [[CrossRef](#)]
40. Takiguchi, K.; Wakabayashi, Y.K.; Irie, H.; Krockenberger, Y.; Otsuka, T.; Sawada, H.; Nikolaev, S.A.; Das, H.; Tanaka, M.; Taniyasu, Y.; et al. Quantum transport evidence of Weyl fermions in an epitaxial ferromagnetic oxide. *Nat. Commun.* **2020**, *11*, 4969. [[CrossRef](#)] [[PubMed](#)]
41. Lin, W.; Liu, L.; Liu, Q.; Li, L.; Shu, X.; Li, C.; Xie, Q.; Jiang, P.; Zheng, X.; Guo, R.; et al. Electric Field Control of the Magnetic Weyl Fermion in an Epitaxial SrRuO<sub>3</sub> (111) Thin Film. *Adv. Mater.* **2021**, *33*, 2101316. [[CrossRef](#)] [[PubMed](#)]
42. Toyoda, S.; Yamada, R.; Kaneko, Y.; Tokura, Y.; Ogawa, N. Weyl fermions in SrRuO<sub>3</sub> detected by Brillouin light scattering. *Appl. Phys. Lett.* **2022**, *120*, 242408. [[CrossRef](#)]
43. Sur, S.; Nandkishore, R. Instabilities of Weyl loop semimetals. *New J. Phys.* **2016**, *18*, 115006. [[CrossRef](#)]
44. Amitani, T.; Nishida, Y. Dynamical chiral magnetic current and instability in Weyl semimetals. *Phys. Rev. B* **2023**, *107*, 014302. [[CrossRef](#)]
45. Yadav, N.; Deo, N. Magnetotransport in Weyl semimetal with and without disorder and the effect of tilted magnetic field. *Phys. E Low-Dimens. Syst. Nanostruct.* **2023**, *148*, 115601. [[CrossRef](#)]
46. Sukhachov, P.O.; Gorbar, E.V.; Shovkovy, I.A. Entropy Wave Instability in Dirac and Weyl Semimetals. *Phys. Rev. Lett.* **2021**, *127*, 176602. [[CrossRef](#)] [[PubMed](#)]
47. Xue, F.; Zhang, X.-X. Instability and topological robustness of Weyl semimetals against Coulomb interaction. *Phys. Rev. B* **2017**, *96*, 195160. [[CrossRef](#)]
48. Boettcher, I. Interplay of Topology and Electron-Electron Interactions in Rarita-Schwinger-Weyl semimetals. *Phys. Rev. Lett.* **2020**, *124*, 127602. [[CrossRef](#)] [[PubMed](#)]
49. Li, T.; Du, G.; Zhang, B.; Zeng, Z. Scaling behavior of hysteresis in multilayer MoS<sub>2</sub> field effect transistors. *Appl. Phys. Lett.* **2014**, *105*, 093107.
50. Park, Y.; Baac, H.W.; Heo, J.; Yoo, G. Thermally activated trap charges responsible for hysteresis in multilayer MoS<sub>2</sub> field-effect transistors. *Appl. Phys. Lett.* **2016**, *108*, 083102. [[CrossRef](#)]
51. Illarionov, Y.Y.; Rzepa, G.; Waltl, M.; Knobloch, T.; Grill, A.; Furchi, M.M.; Mueller, T.; Grasser, T. The role of charge trapping in MoS<sub>2</sub>/SiO<sub>2</sub> and MoS<sub>2</sub>/hBN field-effect transistors. *2D Mater.* **2016**, *3*, 035004. [[CrossRef](#)]
52. Illarionov, Y.Y.; Knobloch, T.; Waltl, M.; Rzepa, G.; Pospischil, A.; Polyushkin, D.A.; Furchi, M.M.; Mueller, T.; Grasser, T. Energetic mapping of oxide traps in double-gated MoS<sub>2</sub> field-effect transistors. *2D Mater.* **2017**, *4*, 025108. [[CrossRef](#)]
53. Knobloch, T.; Rzepa, G.; Illarionov, Y.Y.; Waltl, M.; Schanovsky, F.; Stampfer, B.; Furchi, M.; Mueller, T.; Grasser, T. A Physical Model for the Hysteresis in MoS<sub>2</sub> Transistors. *J. Electr. Dev. Soc.* **2018**, *6*, 972–978. [[CrossRef](#)]

**Disclaimer/Publisher's Note:** The statements, opinions and data contained in all publications are solely those of the individual author(s) and contributor(s) and not of MDPI and/or the editor(s). MDPI and/or the editor(s) disclaim responsibility for any injury to people or property resulting from any ideas, methods, instructions or products referred to in the content.